

Lattice QCD form factor for $B_s \rightarrow D_s^* \ell \nu$ at zero recoil with non-perturbative current renormalisation

E. McLean,^{1,*} C. T. H. Davies,^{1,†} A. T. Lytle,² and J. Koponen³
(HPQCD collaboration),[‡]

¹*SUPA, School of Physics and Astronomy, University of Glasgow, Glasgow, G12 8QQ, UK*

²*INFN, Sezione di Roma Tor Vergata, Via della Ricerca Scientifica 1, 00133 Roma RM, Italy*

³*High Energy Accelerator Research Organisation (KEK), Tsukuba 305-0801, Japan*

(Dated: June 3, 2019)

We present details of a lattice QCD calculation of the $B_s \rightarrow D_s^*$ axial form factor at zero recoil using the Highly Improved Staggered Quark (HISQ) formalism on the second generation MILC gluon ensembles that include up, down, strange and charm quarks in the sea. Using the HISQ action for all valence quarks means that the lattice axial vector current that couples to the W can be renormalized fully non-perturbatively, giving a result free of the perturbative matching errors that previous lattice QCD calculations have had. We calculate correlation functions at three values of the lattice spacing, and multiple ' b '-quark masses, for physical c and s . The functional dependence on the b -quark mass can be determined and compared to Heavy Quark Effective Theory expectations, and a result for the form factor obtained at the physical value of the b -quark mass. We find $\mathcal{F}^{B_s \rightarrow D_s^*}(1) = h_{A_1}^s(1) = 0.9020(96)_{\text{stat}}(90)_{\text{sys}}$. This is in agreement with earlier lattice QCD results, which use NRQCD b quarks, with a total uncertainty reduced by more than a factor of two. We discuss implications of this result for the $B \rightarrow D^*$ axial form factor at zero recoil and for determinations of V_{cb} .

I. INTRODUCTION

The study of quark flavour-changing interactions is a key component of the search for physics beyond the Standard Model (SM). There are currently a number of related tensions between experimental measurements and SM predictions [1–19], along with discrepancies between systematically independent determinations of Cabibbo-Kobayashi-Maskawa (CKM) matrix elements [20–22]. A more precise understanding of these processes is needed to resolve these issues.

The $\bar{B}^0 \rightarrow D^{*+} \ell^- \bar{\nu}$ decay (and its charge conjugate, that we simply abbreviate to $B \rightarrow D^* \ell \nu$ from now on) supplies one of the three methods used for precisely determining the CKM element $|V_{cb}|$ [23–40]. Measurements of branching fractions are extrapolated through q^2 to the zero recoil point to deduce $\mathcal{F}(1)|V_{cb}|$, where $\mathcal{F}(1)$ is the value of the only form factor contributing at zero recoil. Then a determination of $\mathcal{F}(1)$ in the Standard Model (via Lattice QCD [39, 41]) can be divided out to infer $|V_{cb}|$.

$|V_{cb}|$ is an important quantity and needs to be determined accurately. It constrains one side of the unitarity triangle via the ratio $|V_{ub}|/|V_{cb}|$. It is also a dominant uncertainty in the determination of the CP -violation parameter ϵ_K (where there is currently tension between the SM and experiment, see for example [42]).

Previous determinations of $|V_{cb}|$ have shown systematic discrepancies with each other. The two competing values were those derived from *exclusive* decays ($B \rightarrow D^* \ell \nu$

and $B \rightarrow D \ell \nu$ with $B \rightarrow D^*$ giving the more accurate result), and *inclusive* ($B \rightarrow X_c \ell \nu$, where X_c is any charmed hadronic state). In 2016 the Heavy Flavour Averaging Group (HFLAV) gave a value derived from exclusive $B \rightarrow D^*$ decays of $|V_{cb}|_{\text{excl}} = (39.05 \pm 0.47_{\text{exp}} \pm 0.58_{\text{th}}) \times 10^{-3}$ and from inclusive decays, using the kinetic scheme, of $|V_{cb}|_{\text{incl}} = (42.19 \pm 0.78) \times 10^{-3}$ [20]. It has since been suggested, based on unfolded Belle data [38], that the tension seen here arose (at least partly) from the use of a very constrained parameterization in the extrapolation of the experimental $B \rightarrow D^*$ decay rates to zero recoil [43–45]. Recent exclusive determinations of V_{cb} have then used a less constrained parameterisation to give a larger, and less precise, result for V_{cb} that is no longer in tension with the inclusive result. For example, the Particle Data Group quote $|V_{cb}|_{\text{excl}} = (41.9 \pm 2.0) \times 10^{-3}$ [46]. However, an even more recent V_{cb} determination from $B \rightarrow D^* \ell \nu$ data by the BaBar collaboration [47] used the less constrained parameterisation but still found a tension with the inclusive result. This clearly points to the need for more work to improve the accuracy of the exclusive result. On the theory side a better understanding of the form factors for $B \rightarrow D^*$ from lattice QCD is required, both at zero recoil and away from zero recoil.

Another motivation for studying $B \rightarrow D^* \ell \nu$ is the tension between SM and experimental determinations of the ratio $R_{D^{(*)}} = \mathcal{B}(\bar{B} \rightarrow D^{(*)} \tau \bar{\nu}_\tau) / \mathcal{B}(\bar{B} \rightarrow D^{(*)} \ell \bar{\nu}_\ell)$ ($\ell = e$ or μ). The latest HFLAV report gives the combined statistical significance of the anomalies in R_D and R_{D^*} to be 3.8σ [20]. A preliminary new analysis from Belle [48], however, gives results closer to the SM and pulls the global average down to 3.1σ . More precise measurements and predictions will either confirm or dismiss a new physics explanation.

The weak decay process $B_s \rightarrow D_s^* \ell \nu$ is very similar

*e.mclean.1@research.gla.ac.uk

†christine.davies@glasgow.ac.uk

‡URL: <http://www.physics.gla.ac.uk/HPQCD>

to $B \rightarrow D^* \ell \nu$ and could also be used to determine $|V_{cb}|$ and test the SM. It is feasible to study this decay at LHC and from the theoretical side it is a more attractive channel than $B \rightarrow D^*$. The absence of valence light quarks means that lattice QCD results have smaller statistical errors and are less computationally expensive. Finite-volume effects and the dependence on u/d quark masses (for quarks in the sea) are also smaller. The D_s^* has no Zweig-allowed strong decay mode, unlike the D^* , and is in fact a relatively long-lived particle [49] that can be considered ‘gold-plated’ in lattice QCD. This makes the $B_s \rightarrow D_s^* \ell \nu$ both a useful test bed for lattice techniques (that may be later used to study $B \rightarrow D^* \ell \nu$ decays) and a key decay process for which to make predictions ahead of experimental results.

Lattice QCD calculations have shown that several weak decay form factors are relatively insensitive to whether the spectator quark is a u/d or s quark [50–52]. A combination of chiral perturbation theory and Heavy Quark Symmetry [53] backs up this expectation for B decays. We can therefore expect the form factors to be very similar for $B_s \rightarrow D_s^*$ and $B \rightarrow D^*$. A recent lattice calculation [41] found an insignificant $\mathcal{O}(1\%)$ difference at zero recoil: $\mathcal{F}^{B \rightarrow D^*}(1)/\mathcal{F}^{B_s \rightarrow D_s^*}(1) = 1.013(14)_{\text{stat}}(17)_{\text{sys}}$. Information from the study of $B_s \rightarrow D_s^*$ can then be applicable to $B \rightarrow D^*$.

Lattice QCD calculations of the $B_{(s)} \rightarrow D_{(s)}^*$ form factors at zero recoil have so far been performed by two collaborations using different methods. The Fermilab Lattice and MILC collaborations calculated $\mathcal{F}^{B \rightarrow D^*}(1)$ in [39, 54] using the Fermilab action for both b and c quarks [55] and asqtad u/d quarks [56]. More recently the HPQCD collaboration computed both $\mathcal{F}^{B \rightarrow D^*}(1)$ and $\mathcal{F}^{B_s \rightarrow D_s^*}(1)$ [41] using improved NRQCD b quarks [57, 58] and Highly Improved Staggered (HISQ) c and $u/d/s$ quarks [59]. The RBC/UKQCD [60] and LANL-SWME [61] collaborations are also working towards these form factors using variants of the Fermilab action for heavy quarks and JLQCD has a calculation in progress using Möbius domain-wall quarks [62].

The formalism to use for the heavy quarks is a major consideration in designing a lattice QCD calculation to determine these form factors. Most of the calculations discussed in the previous paragraph (apart from the JLQCD calculation) use approaches that make use of the nonrelativistic nature of heavy quark bound states to tune the b (and in some cases also c) quark masses. This avoids potentially large discretisation effects appearing in the results in the form of a systematic error of size $(am_b)^n$, where n is an integer that depends on the level of improvement in the action. The absence of these discretisation errors means that b quarks can be handled on relatively coarse lattices where $am_b > 1$. However the price to be paid is that the current operator that couples to the W boson is also implemented within a non-relativistic framework and must then be renormalised to match the appropriate operator in continuum QCD. This matching can be done using perturbative lattice QCD but

has only been done through $\mathcal{O}(\alpha_s)$ for these actions [63, 64]. This leaves a substantial source of uncertainty from missing higher-order terms in the perturbative matching that is not easily reduced. This matching uncertainty contributes $\sim 80\%$ of the final error in the HPQCD calculation [41] and $\sim 30\%$ in the Fermilab/MILC calculation [39] because of the differing allowances for missing higher-order terms.

Here we report details and results of a calculation of the $B_s \rightarrow D_s^*$ form factor at zero recoil using an approach free of perturbative matching uncertainties. We perform our calculation on the second-generation MILC ensembles [65, 66], including effects from 2+1+1 flavours in the sea using the HISQ action. We also use the HISQ action for all valence quarks. We obtain results at a number of differing masses for the b (we refer to this generically as the *heavy quark* h), and perform an extrapolation to $m_h = m_b$. By using only HISQ quarks, we can obtain the normalizations of all required currents fully non-perturbatively. We refer to this as the *heavy-HISQ* approach. By using many heavy masses and multiple values of the lattice spacing, including very fine lattices, we can model both the form factor dependence on the heavy mass, and the discretisation effects associated with using large am_h values.

The heavy-HISQ approach was developed by HPQCD to compute B meson masses and decay constants [67, 68] and the b quark mass [69, 70]. It is also now being used by other collaborations for these calculations [71, 72]. A proof-of-principle application of heavy-HISQ to form factors was given in [73, 74] for B_c decays, showing that the full q^2 range of the decay could be covered. Here we extend the approach to form factors for B_s decays but working only at zero recoil, a straightforward extension of earlier work. Using the heavy-HISQ approach also has the added benefit of elucidating the dependence of form factors on heavy quark masses, meaning that we can test expectations from Heavy Quark Effective Theory (HQET).

This article is structured in the following way: Section II defines the form factor and gives details of the lattice calculation, including the nonperturbative normalisation and extrapolation in heavy-quark mass; Section III presents our results and compares to earlier calculations and Section IV gives our conclusions and outlook. In the appendix, we give details of a number of tests we performed on the correlator fits and the continuum, chiral and heavy-quark extrapolations.

II. CALCULATION DETAILS

A. Form Factors

The differential decay rate for the $\bar{B}_s^0 \rightarrow D_s^{*+} l^- \bar{\nu}_l$ decay is given in the SM by

$$\frac{d\Gamma}{dw}(\bar{B}_s^0 \rightarrow D_s^{*+} l^- \bar{\nu}_l) = \frac{G_F^2 M_{D_s^*}^3 |\bar{\eta}_{EW} V_{cb}|^2}{4\pi^3} \times (M_{B_s}^2 - M_{D_s^*}^2) \sqrt{w^2 - 1} \chi(w) |\mathcal{F}^{B_s \rightarrow D_s^*}(w)|^2. \quad (1)$$

where $w = v_{B_s} \cdot v_{D_s^*}$, $v = p/M$ is the 4-velocity of each meson, and $\chi(w)$ is a known function of w with $\chi(1) = 1$ (see, for example, appendix G of [41]). $\bar{\eta}_{EW}$ accounts for electroweak corrections from diagrams where photons or Z s are exchanged in addition to a W^- , as well as the Coulomb attraction of the final-state charged particles [75–77]. The differential decay rate for the $B_s^0 \rightarrow D_s^{*-} l^+ \nu_l$ is identical.

The form factor $\mathcal{F}^{B_s \rightarrow D_s^*}(w)$ is a linear combination of hadronic form factors that parameterize the vector and axial-vector matrix elements between initial and final state hadrons. A common choice of parameterization used in the context of Heavy Quark Effective Theory (HQET) is [78]

$$\langle D_s^*(\epsilon) | V^\mu | B_s \rangle = i \sqrt{M_{B_s} M_{D_s^*}} h_V^s(w) \epsilon_{\mu\nu\alpha\beta} \epsilon^{*\nu} v_{D_s^*}^\alpha v_{B_s}^\beta, \quad (2)$$

$$\langle D_s^*(\epsilon) | A^\mu | B_s \rangle = \sqrt{M_{B_s} M_{D_s^*}} [h_{A_1}^s(w)(w+1)\epsilon_\mu^* - h_{A_2}^s(w)\epsilon^* \cdot v_{B_s} v_{B_s\mu} - h_{A_3}^s(w)\epsilon^* \cdot v_{B_s} v_{D_s^*\mu}], \quad (3)$$

where $V^\mu = \bar{c}\gamma^\mu b$ is the vector $b \rightarrow c$ current and $A^\mu = \bar{c}\gamma^\mu\gamma^5 b$ is the axial-vector current. ϵ is the polarization 4-vector of the D_s^* final state.

At zero recoil ($w = 1$), the vector matrix element vanishes, the axial-vector element simplifies to

$$\langle D_s^*(\epsilon) | A^\mu | B_s \rangle = 2\sqrt{M_{B_s} M_{D_s^*}} h_{A_1}^s(1) \epsilon^{*\mu}, \quad (4)$$

and $\mathcal{F}^{B_s \rightarrow D_s^*}(w)$ reduces to

$$\mathcal{F}^{B_s \rightarrow D_s^*}(1) = h_{A_1}^s(1). \quad (5)$$

Our goal is to compute $h_{A_1}^s(1)$.

All we need to do this is the matrix element $\langle D_s^*(\epsilon) | A^\mu | B_s \rangle$ with both the B_s and D_s^* at rest, with the D_s^* polarization ϵ in the same direction as the (spatial) axial-vector current.

B. Lattice Calculation

The gluon field configurations that we use were generated by the MILC collaboration [65, 66]. Table I gives the relevant parameters for the specific ensembles that we use. The gluon field is generated using a

Symanzik-improved gluon action with coefficients calculated through $\mathcal{O}(\alpha_s a^2, n_f \alpha_s a^2)$ [79]. The configurations include the effect of 2+1+1 flavours of dynamical quarks in the sea (u, d, s, c , with $m_u = m_d \equiv m_l$), using the HISQ action [59]. In three of the four ensembles (fine, superfine and ultrafine), the bare light quark mass is set to $m_{l0}/m_{s0} = 0.2$. The fact that the m_{l0} value is unphysically high is expected to have only a small effect on $h_{A_1}^s(1)$, because there are no valence light quarks. The effect is quantified here by including a fourth ensemble (fine-physical) with (approximately) physical m_{l0} .

We use a number of different masses for the valence heavy quark, h . This is in order to resolve the dependence of $h_{A_1}^s(1)$ on the heavy mass, so that an extrapolation to $m_h = m_b$ can be performed. By varying the heavy mass on each ensemble and by using ensembles at varying small lattice spacing, we can resolve both the discretisation effects that grow with heavy quark mass ($am_{h0}^{\text{val}} \lesssim 1$) and the physical dependence of the continuum form factor on m_h .

Staggered quarks have no spin degrees of freedom, so that solution of the Dirac equation on each gluon field is numerically fast. The remnant of the doubling problem means that quark bilinears of specific spin-parity have multiple copies, called ‘tastes’ [59]. They differ in the amount of point-splitting between the fields and the space-time dependent phase needed to substitute for the appropriate γ matrix. In this calculation we can use only local (non point-split) bilinears, which is an advantage in terms of statistical noise, since no gluon fields are included in the current operator. In the standard staggered spin-taste notation, the operators that we use are: pseudoscalar, $\Gamma_P = (\gamma^5 \otimes \gamma^5)$; vector, $\Gamma_V^\mu = (\gamma^\mu \otimes \gamma^\mu)$ and axial-vector, $\Gamma_A^\mu = (\gamma^\mu \gamma^5 \otimes \gamma^\mu \gamma^5)$.

We compute several ‘two-point’ correlation functions on the ensembles detailed in table I, combining HISQ propagators from solving the Dirac equation for each random wall time source. These correlation functions take the form

$$C_M(t) = \frac{1}{N_{\text{taste}}} \langle \Phi_M(t) \Phi_M^\dagger(0) \rangle, \quad (6)$$

$$\Phi_M(t) = \sum_{\mathbf{x}} \bar{q}(\mathbf{x}, t) \Gamma q'(\mathbf{x}, t),$$

where $\langle \rangle$ represents a functional integral, q, q' are valence quark fields of the flavours the M meson is charged under, Γ is the spin-taste structure of M and $1/N_{\text{taste}}$ is the staggered quark normalisation for closed loops. The random-wall source and the sum over \mathbf{x} at the sink project onto zero spatial momentum. We compute the correlation functions for all t values, i.e. $0 \leq t \leq N_t$.

The correlation function for the heavy-strange pseudoscalar meson, H_s , with valence quark content $h\bar{s}$ and spin-taste structure Γ_P is constructed from HISQ propagators as:

$$C_{H_s}(t) = \frac{1}{4} \sum_{\mathbf{x}, \mathbf{y}} \text{Tr} [g_h(x, y) g_s^\dagger(x, y)]. \quad (7)$$

| set | handle | w_0/a | $N_x^3 \times N_t$ | $n_{\text{cfg}} \times n_{\text{src}}$ | am_{l0} | am_{s0} | am_{c0} | am_{s0}^{val} | am_{c0}^{val} | am_{h0}^{val} | T |
|-----|----------------------|------------|--------------------|--|-----------|-----------|-----------|------------------------|------------------------|-------------------------|----------|
| 1 | fine | 1.9006(20) | $32^3 \times 96$ | 938×8 | 0.0074 | 0.037 | 0.440 | 0.0376 | 0.45 | 0.5, 0.65, 0.8 | 14,17,20 |
| 2 | fine-physical | 1.9518(7) | $64^3 \times 96$ | 284×4 | 0.0012 | 0.0363 | 0.432 | 0.036 | 0.433 | 0.5, 0.8 | 14,17,20 |
| 3 | superfine | 2.896(6) | $48^3 \times 144$ | 250×8 | 0.0048 | 0.024 | 0.286 | 0.0234 | 0.274 | 0.427, 0.525, 0.65, 0.8 | 22,25,28 |
| 4 | ultrafine | 3.892(12) | $64^3 \times 192$ | 249×4 | 0.00316 | 0.0158 | 0.188 | 0.0165 | 0.194 | 0.5, 0.65, 0.8 | 31,36,41 |

TABLE I: Parameters for the ensembles of gluon field configurations that we use [65, 66]. a is the lattice spacing, determined from the Wilson flow parameter, w_0 . Values for w_0/a are from: set 1, [80], sets 2 and 3, [70] and set 4 [81]. The physical value of w_0 was determined at 0.1715(9) fm from f_π [82]. N_x is the spatial extent and N_t the temporal extent of the lattice in lattice units; n_{cfg} is the number of gluon field configurations in the ensemble and n_{src} the number of different time sources used per configuration. Light, strange and charm quarks are included in the sea, their masses are given in columns 6-8, and the valence quark masses in columns 9-11. The s and c valence quarks were tuned in [70]. We use a number of heavy quark masses to assist the extrapolation to the physical b mass. Column 12 gives the temporal separations between source and sink, T , of the 3-point correlation functions computed on each ensemble.

Here $g_q(x, y)$ is a HISQ propagator for flavour q , the trace is over color and $1/4$ is the staggered quark normalisation. $x_0 = 0$ and $y_0 = t$ and the sum is over spatial sites \mathbf{x}, \mathbf{y} . We also compute correlators for a charm-strange vector meson D_s^* , with structure Γ_V^i , using

$$C_{D_s^*}(t) = \frac{1}{4} \sum_{\mathbf{x}, \mathbf{y}} (-1)^{x_i + y_i} \text{Tr} [g_c(x, y) g_s^\dagger(x, y)]. \quad (8)$$

We average over polarisations, $i = 1, 2, 3$.

We also compute correlation functions for two tastes of pseudoscalar heavy-charm mesons denoted H_c and \hat{H}_c respectively. H_c has spin-taste structure Γ_P , and \hat{H}_c has structure Γ_A^0 . H_c correlators are computed using Eq. (7) (with g_s replaced with g_c), while \hat{H}_c correlators are given by

$$C_{\hat{H}_c}(t) = \frac{1}{4} \sum_{\mathbf{x}, \mathbf{y}} (-1)^{\bar{x}_0 + \bar{y}_0} \text{Tr} [g_h(x, y) g_c^\dagger(x, y)], \quad (9)$$

where we use the notation $\bar{z}_\mu = \sum_{\nu \neq \mu} z_\nu$. These correlators will be used to normalise the axial vector $b\bar{c}$ current as discussed in Section II D.

A useful physical proxy (that does not run) for the quark mass is that of the pseudoscalar meson made from that flavour of quark. It is therefore also useful, for our heavy quark mass extrapolation, to calculate correlation functions for heavy-heavy pseudoscalars, denoted η_h , with spin-taste structure Γ_P using Eq. (7). Likewise, to test the impact of any mistuning of the charm and strange quark masses, we also determine η_c and η_s correlators analogously. We can tune the c and b masses using the experimental values for the η_c and η_b masses, allowing for slight shifts from missing QED effects and the fact that we do not allow these mesons to annihilate to gluons [69]. The mass of the η_s meson (which is not a physical state) can be fixed in lattice QCD from the K and π meson masses [82, 83].

We then generate the ‘three-point’ correlation func-

tions that contain the H_s to D_s^* transition.

$$C_{3\text{pt}}(t, T) = \frac{1}{N_{\text{taste}}} \sum_{\mathbf{y}} \langle \Phi_{D_s^*}(T) A^i(\mathbf{y}, t) \Phi_{H_s}(0) \rangle, \quad (10)$$

$$A^\mu(\mathbf{y}, t) = \bar{c}(\mathbf{y}, t) \gamma^5 \gamma^\mu h(\mathbf{y}, t).$$

Our H_s source is given spin-taste Γ_P , the D_s^* sink, Γ_V^i , and the current insertion Γ_A^i . This gives the required cancellation of tastes within the three-point function [84]. In terms of HISQ propagators

$$C_{3\text{pt}}(t, T) = \frac{1}{4} \sum_{\mathbf{x}, \mathbf{y}, \mathbf{z}} (-1)^{\bar{y}_i + \bar{z}_i} \times \text{Tr} [g_h(x, y) g_c(y, z) g_s^\dagger(z, x)], \quad (11)$$

where we fix $x_0 = 0$, $y_0 = t$ and $z_0 = T$. We compute the three-point correlation functions for all t values within $0 \leq t \leq T$, and 3 T values that vary between ensembles and are given in Table I. We average over the 3 directions for i for increased statistical precision.

C. Analysis of Correlation Functions

We use simultaneous Bayesian fits [85, 86] to extract the axial vector matrix element and meson masses from the two- and three-point correlation functions. This allows us to include the covariance between results at different heavy quark masses on a given ensemble into our subsequent fits in Section II E.

We fit the two-point correlation functions using the functional form

$$C_M(t)|_{\text{fit}} = \sum_n^{N_{\text{exp}}} \left(|a_n^M|^2 f(E_n^M, t) - (-1)^t |a_n^{M,o}|^2 f(E_n^{M,o}, t) \right); \quad (12)$$

$$f(E, t) = \left(e^{-Et} + e^{-E(N_t - t)} \right),$$

where N_t is the temporal extent of the lattice, and $E_n^{M,(o)}, a_n^{M,(o)}$ are fit parameters, with the excited-state energy parameters implemented as energy differences to the state below [85]. The second term accounts for the presence of opposite-parity states that contribute an oscillating term to the correlation function when using staggered quarks [59]. These terms do not appear when M is a pseudoscalar with a quark and antiquark of the same mass, so in the $M = \eta_h, \eta_c$, and η_s cases the second term is not required. For all correlator fits we set $N_{\text{exp}} = 5$; this allows the impact of systematic effects from excited states to be included in the ground-state parameters that we are interested in.

The three-point correlation functions have the fit form

$$C_{3\text{pt}}(t, T)|_{\text{fit}} = \sum_{k,j=0}^{N_{\text{exp}}, N_{\text{exp}}} \quad (13)$$

$$\begin{aligned} & \left(a_j^{H_s} J_{jk}^{nn} a_k^{D_s^*} f(E^{H_s}, t) f(E_n^{D_s^*}, T-t) \right. \\ & + a_j^{H_s, o} J_{jk}^{on} a_k^{D_s^*} (-1)^t f(E_n^{H_s, o}, t) f(E^{D_s^*}, T-t) \\ & + a_j^{H_s} J_{jk}^{no} a_k^{D_s^{*, o}} (-1)^{T-t} f(E^{H_s}, t) f(E_n^{D_s^{*, o}}, T-t) \\ & \left. + a_j^{H_s, o} J_{jk}^{oo} a_k^{D_s^{*, o}} (-1)^T f(E_n^{H_s, o}, t) f(E^{D_s^{*, o}}, T-t) \right). \end{aligned}$$

This includes fit parameters common to the fits of the H_s and D_s^* two-point correlators, along with new fit parameters J_{jk} .

We perform a single simultaneous fit containing each correlator computed ($H_s, D_s^*, \eta_h, \eta_c, \eta_s, H_c, \hat{H}_c$, and three-point) for each ensemble. We set gaussian priors for the parameters J_{jk} , and log-normal priors for all other parameters. Using log-normal distributions forbids energy differences $E_{n+1}^M - E_n^M$ and amplitudes a_n^M (which can be taken to be positive here) from moving too close to zero or changing sign, improving stability of the fit.

Ground state energies E_0^M are given priors of $(am_{q0} + am_{q'0} + a\Lambda_{\text{QCD}}) \pm 2a\Lambda_{\text{QCD}}$, where m_{q0} and $m_{q'0}$ are the masses of the appropriate quarks, and Λ_{QCD} is the confinement scale, which we set to 0.5 GeV. For $q = h$ or c , this corresponds to the leading order HQET expression for a heavy meson mass. Ground-state energies of oscillating states, $E_0^{M,o}$, are given priors of $(am_{q0} + am_{q'0} + 2a\Lambda_{\text{QCD}}) \pm 2a\Lambda_{\text{QCD}}$. Excited state energy differences, $E_{i+1}^M - E_i^M$, $i > 0$ are given prior values $2a\Lambda_{\text{QCD}} \pm a\Lambda_{\text{QCD}}$. Priors for ground state amplitudes a_0^M , are set from plots of effective amplitudes. The resulting priors always have a variance at least 10 times that of the final result for the ground-state. We use log(amplitude) priors of -1.20(67) for non-oscillating excited states and -3.0(2.0) for oscillating excited states. The ground-state non-oscillating to non-oscillating 3-point parameter, J_{00}^{nn} is given a prior of 1 ± 0.6 , and the rest of the 3-point parameters J_{jk}^{nn} are given 0 ± 1 .

$E_0^M = aM_M$ is the mass of the ground-state meson M in lattice units. The masses M_{H_s} and M_{η_h} can both be used as proxys for m_h in the extrapolation to $m_h = m_b$.

The annihilation amplitude for an M -meson is given (in lattice units) by

$$\langle 0 | \Phi_M | M \rangle |_{\text{lat}} = \sqrt{2M_M} a_0^M. \quad (14)$$

The (as yet unnormalised) matrix element that we need to obtain $h_{A_1}^s(1)$ is given by

$$\langle D_s^*(\hat{k}) | A^k | H_s \rangle |_{\text{lat}} = 2\sqrt{M_{H_s} M_{D_s^*}} J_{00}^{nn}. \quad (15)$$

To ensure that truncating the sum over states at N_{exp} accounts for the full systematic error from excited states, we cut out some data very close to the sources and sinks, where even higher excited states might have some effect. To do this we only include data with $t \geq t_{\text{cut}}$ and $t \leq N_t - t_{\text{cut}}$ in the two-point case and $t \leq T - t_{\text{cut}}$ in the three-point case. We can in principle use a different t_{cut} for every correlation function included in our fit, but we do not use a big range of t_{cut} values. They range from 1 to 3 for the three-point functions and up to 8 for the two-point functions.

The determination and minimisation of the χ^2 function in our fit procedure requires the inversion of the covariance matrix that captures correlations between the different pieces of ‘data’ (correlation functions) in our fit. The low eigenmodes of the correlation matrix are not well determined with the statistics that we have and so we implement an SVD (singular value decomposition) cut in the inversion of the correlation matrix to avoid underestimating the uncertainty in the parameters of the fit [86]. This replaces correlation matrix eigenvalues below λ_{min} , equal to svdcut times the largest eigenvalue, with λ_{min} . λ_{min} is estimated using the diagnosis tools in the Corrfitter package [86] and corresponds typically to an svdcut of 10^{-3} here.

Figure 1 summarises stability tests of our fits, focussing on the key parameter J_{00}^{nn} that is converted to the ground-state to ground-state transition amplitude using Eq. (15).

The fit parameters determined by our fits that we will use to calculate the physical value for $h_{A_1}^s(1)$ are given in Table II. Notice that the statistical errors on the results grow with the heavy quark mass. This is a well understood problem in lattice heavy-light meson physics (see, for example [87]). Our method here has the advantage of including information from lighter-than- b heavy quarks with improved statistical precision.

D. Normalisation of the Axial Current

The partially-conserved axial-vector current for the HISQ action is a complicated linear combination of one-link and three-link lattice currents. In this study we use only local axial vector currents. This simplifies the lattice QCD calculation but creates the need for our resulting current matrix element to be multiplied by a matching

| Set | am_{h0}^{val} | $h_{A_1}^s(1)$ | aM_{H_s} | $aM_{D_s^*}$ | aM_{H_c} | af_{H_c} | aM_{η_h} | aM_{η_c} | aM_{η_s} |
|-----|------------------------|----------------|-------------|--------------|--------------|--------------|---------------|---------------|---------------|
| 1 | 0.5 | 0.9255(20) | 0.95972(12) | 0.96616(44) | 1.419515(41) | 0.186299(70) | 1.471675(38) | 1.367014(40) | 0.313886(75) |
| | 0.65 | 0.9321(22) | 1.12511(16) | | 1.573302(40) | 0.197220(77) | 1.775155(34) | | |
| | 0.8 | 0.9434(24) | 1.28128(21) | | 1.721226(39) | 0.207068(78) | 2.064153(30) | | |
| 2 | 0.5 | 0.9231(21) | 0.95462(12) | 0.93976(42) | 1.400034(28) | 0.183472(62) | 1.470095(25) | 1.329291(27) | 0.304826(52) |
| | 0.8 | 0.9402(27) | 1.27577(22) | | 1.702456(23) | 0.203407(45) | 2.062957(19) | | |
| 3 | 0.427 | 0.9107(46) | 0.77453(24) | 0.63589(49) | 1.067224(46) | 0.126564(70) | 1.233585(41) | 0.896806(48) | 0.207073(96) |
| | 0.525 | 0.9165(49) | 0.88487(31) | | 1.172556(46) | 0.130182(72) | 1.439515(37) | | |
| | 0.65 | 0.9246(65) | 1.02008(39) | | 1.303144(46) | 0.133684(75) | 1.693895(33) | | |
| | 0.8 | 0.9394(66) | 1.17487(54) | | 1.454205(46) | 0.137277(79) | 1.987540(30) | | |
| 4 | 0.5 | 0.9143(51) | 0.80245(24) | 0.47164(39) | 1.011660(32) | 0.098970(52) | 1.342639(65) | 0.666586(89) | 0.15412(17) |
| | 0.65 | 0.9273(62) | 0.96386(33) | | 1.169761(34) | 0.100531(60) | 1.650180(56) | | |
| | 0.8 | 0.9422(72) | 1.11787(43) | | 1.321647(37) | 0.101714(70) | 1.945698(48) | | |

TABLE II: Values extracted from correlation function fits for $h_{A_1}^s(1)$, along with quantities required in our fits to determine a value at the physical point. Results are given on each gluon field ensemble for each valence heavy quark mass used. Results come from our simultaneous fits to two-point and three-point correlation functions: $h_{A_1}^s(1)$ values are determined using Eq. (19) and the ground-state meson masses in columns 4, 5, 6, 8, 9 and 10 from Eq. (12). f_{H_c} is the H_c meson decay constant determined from Eq. (A1).

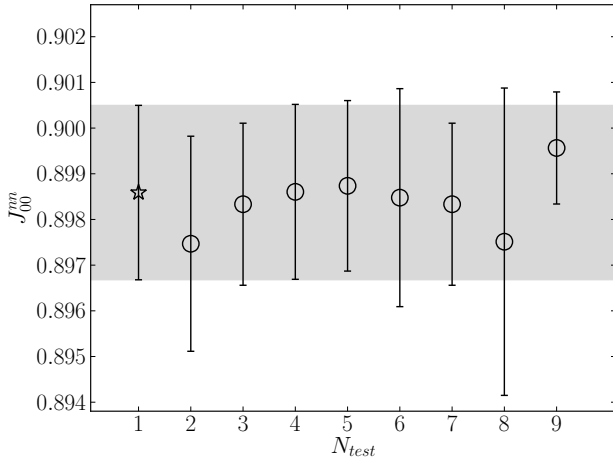


FIG. 1: Tests of the stability of correlator fits for J_{00}^{nn} from fitting the two- and three-point correlators at heavy mass $am_{h0}^{\text{val}} = 0.5$ on the fine ensemble. $N_{\text{test}} = 1$ gives our final result. $N_{\text{test}} = 2$ gives the results when all priors are broadened by 50%. $N_{\text{test}} = 3$ and 4 give the results of setting $N_{\text{exp}} = 4$ and 6 respectively. $N_{\text{test}} = 5, 6$ give the result of setting $t_{\text{cut}} = 2, 4$ respectively for all correlators. $N_{\text{test}} = 7$ gives the result without marginalising out the $n = 5$ excited state. $N_{\text{test}} = 8$ gives the result of changing the SVD cut from 10^{-3} to 10^{-2} . $N_{\text{test}} = 9$ gives the result from a fit containing only $am_{h0}^{\text{val}} = 0.5$ correlators and hence with a smaller covariance matrix. This allows us, as a test, to use a reduced SVD cut of 10^{-5} .

factor Z_A to produce the appropriate continuum current. We determine Z_A via a fully non-perturbative method [84].

We use the fact that the staggered local pseudoscalar

current of spin-taste ($\gamma^5 \otimes \gamma^5$), multiplied by the sum of its valence quark masses, is absolutely normalized via the PCAC relation. From the two-point H_c and \hat{H}_c correlator fits we can extract the decay amplitudes: $\langle 0 | \bar{c}(\gamma^5 \otimes \gamma^5) h | H_c \rangle \equiv \langle 0 | P | H_c \rangle$ and $\langle 0 | \bar{c}(\gamma^0 \gamma^5 \otimes \gamma^0 \gamma^5) h | \hat{H}_c \rangle = \langle 0 | A^0 | \hat{H}_c \rangle$ as in Eq. (14). Then, the normalization for the local A^0 current (common to that of the local spatial axial-vector current A^k up to discretisation effects), Z_A , is fixed by demanding that

$$(m_{h0}^{\text{val}} + m_{c0}^{\text{val}}) \langle 0 | P | H_c \rangle |_{\text{lat}} = M_{\hat{H}_c} Z_A \langle 0 | A^0 | \hat{H}_c \rangle |_{\text{lat}}. \quad (16)$$

The Z_A values found on each ensemble and am_{h0}^{val} are given in Table III.

There is an ambiguity in what mass to use on the right hand side of Eq. (16). We use the non-goldstone mass $M_{\hat{H}_c}$, but one could just as well replace this with M_{H_c} since the difference is a discretisation effect. The meson mass difference is very small for heavy mesons [59] and so we find the effect of changing the taste of meson mass used never exceeds 0.15% of Z_A throughout the range of ensembles and heavy masses that we use and has no impact on the continuum result.

We also remove tree-level mass-dependent discretisation effects coming from the wavefunction renormalisation [59] by multiplying by a factor Z_{disc} . This is derived in [64] as:

$$Z_{\text{disc}} = \sqrt{\tilde{C}_h \tilde{C}_c}, \quad (17)$$

$$\tilde{C}_q = \cosh am_{q,\text{tree}} \left(1 - \frac{1 + \epsilon_{q,\text{Naik}}}{2} \sinh^2 am_{q,\text{tree}} \right).$$

See also [71]. $m_{q,\text{tree}}$ is the tree-level pole mass in the HISQ action. It has an expansion in terms of the bare

| Set | am_{h0}^{val} | Z_A | Z_{disc} |
|-----|------------------------|-------------|-------------------|
| 1 | 0.5 | 1.03178(57) | 0.99819 |
| | 0.65 | 1.03740(58) | 0.99635 |
| | 0.8 | 1.04368(56) | 0.99305 |
| 2 | 0.5 | 1.03184(47) | 0.99829 |
| | 0.8 | 1.04390(39) | 0.99315 |
| 3 | 0.427 | 1.0141(12) | 0.99931 |
| | 0.525 | 1.0172(12) | 0.99859 |
| | 0.65 | 1.0214(12) | 0.99697 |
| | 0.8 | 1.0275(12) | 0.99367 |
| 4 | 0.5 | 1.00896(44) | 0.99889 |
| | 0.65 | 1.01363(49) | 0.99704 |
| | 0.8 | 1.01968(55) | 0.99375 |

TABLE III: Normalization constants applied to the lattice axial vector current in (19). Z_A is found from (16) and Z_{disc} from (17).

mass [59]

$$am_{q,\text{tree}} = am_{q0} \left(1 - \frac{3}{80} am_{q0}^4 + \frac{23}{2240} am_{q0}^6 \right. \quad (18)$$

$$\left. + \frac{1783}{537600} am_{q0}^8 - \frac{76943}{23654400} am_{q0}^{10} + \mathcal{O}(am_{q0}^{12}) \right),$$

$\epsilon_{q,\text{Naik}}$ fixes the Naik parameter [88] ($N = 1 + \epsilon$ is the coefficient of the tree-level improvement term for the derivative) in the HISQ action when it is being used for heavy quarks [59]. $\epsilon_{q,\text{Naik}}$ is set to its tree-level value, removing the leading tree-level errors from the dispersion relation. As an expansion in $am_{q,\text{tree}}$ it begins at $\mathcal{O}(am_{q,\text{tree}})^2$ [59]. To determine $\epsilon_{q,\text{Naik}}$ we use the closed form expression for it given in [64] and this can also be used along with Eq. (18) to evaluate Z_{disc} . The pole condition can be used to show that the expansion of \tilde{C}_q begins at am_{q0}^4 as $1 - 3am_{q0}^4/80 + \dots$. The effect of Z_{disc} is then very small, never exceeding 0.2%. Z_{disc} values on each ensemble for each am_{h0}^{val} are given in table III.

Combining these normalizations with the lattice current from the 3-point fits, we find a value for the form factor at a given heavy mass and lattice spacing:

$$h_{A_1}^s(1) = \frac{1}{3} \sum_{k=1}^3 \frac{Z_A Z_{\text{disc}} \langle D_s^*(\hat{k}) | A^k | H_s \rangle_{\text{lat}}}{2\sqrt{M_{H_s} M_{D_s^*}}}. \quad (19)$$

E. Obtaining a Result at the Physical Point

We now discuss how we fit our results for the zero recoil form factor, $h_{A_1}^s(1)$, as a function of valence heavy quark mass, sea light quark mass and lattice spacing to obtain a result at the physical point where the heavy quark mass is that of the b , the sea quark masses are physical and the lattice spacing is zero.

In summary, we fit our results for $h_{A_1}^s(1)$ to the following form

$$h_{A_1}^s(1)(a, m_l, m_h) = 1 - \left(\frac{\epsilon_c}{2}\right)^2 l_V + \epsilon_c \epsilon_h \frac{l_A}{2} - \left(\frac{\epsilon_h}{2}\right)^2 l_P \quad (20)$$

$$+ \mathcal{N}_{\text{disc}} + \mathcal{N}_{\text{mistuning}}.$$

The terms in the first line allow for dependence on the valence heavy quark and charm quark masses (with $\epsilon_q \equiv 1/m_q$) using input from HQET, to be discussed below. $\mathcal{N}_{\text{disc}}$ and $\mathcal{N}_{\text{mistuning}}$ account for discretisation and mass mistuning effects, also discussed below. The physical result is then $h_{A_1}^s(1)(0, m_{l,\text{phys}}, m_b)$.

1. Dependence on the heavy valence quark mass

Our fit of the m_h dependence is guided by HQET, which considers both the c quark and the heavy quark of mass m_h to be heavy here. In particular, for the parameter $h_{A_1}^{(s)}(1)$, HQET forbids terms of $\mathcal{O}(1/m_Q)$ where m_Q can be m_c or m_b [89]. The HQET expression for $h_{A_1}(1)$ is then given by [90, 91]:

$$h_{A_1}(1) = \eta_A \left(1 - \frac{l_V}{(2m_c)^2} + \frac{l_A}{2m_c m_h} - \frac{l_P}{(2m_h)^2} \right) \quad (21)$$

$$+ \mathcal{O}\left(\frac{1}{m_c^n m_h^m}, n+m \geq 3\right),$$

where l_V , l_A and l_P are $\mathcal{O}(\Lambda_{\text{QCD}}^2)$ (with possible mild dependence on whether the spectator quark is s or u/d). η_A accounts for ultraviolet matching between HQET and QCD, and has been computed to 2-loops in perturbative QCD [92]. It has mild dependence on m_h through logarithms of m_c/m_h ; at one-loop η_A has explicit form [93]

$$\eta_A = 1 - \frac{\alpha_s}{\pi} \left(\frac{1 + m_c/m_h}{1 - m_c/m_h} \ln \frac{m_c}{m_h} + \frac{8}{3} \right). \quad (22)$$

The coefficient of α_s/π then varies from -0.66 to -0.29 across the range of m_h from $m_h = m_c$ to $m_h = m_b$, taking $m_b/m_c = 4.577(8)$ [94]. The two-loop correction is small [92]. η_A is then close to 1 and differs by a few percent across our range of m_h .

Our calculation has results at multiple values of m_h , and could therefore in principle provide information on the coefficients l_A and l_P of the m_h -dependent terms in the HQET expansion. The charm quark mass is fixed to its physical value and so we cannot access the value of l_V independent of a choice of η_A at $m_h = m_c$. The terms in round brackets in Eq. (21), multiplying η_A , are all very small because of the suppression by heavy-quark masses. To constrain them tightly requires very precise data and, as we will see, we are not able to determine l_A , l_P or l_V accurately with our results. It therefore does not make sense to attempt to compare them accurately to HQET expectations. To do so would require using an appropriate quark mass definition (since different definitions

will move quark mass dependence between the l_A term and the others in Eq. (21) and the two-loop expression for η_A with appropriate value for α_s (since logarithmic m_h dependence of η_A can be misinterpreted as part of a polynomial in $1/m_h$).

Instead we simply take an HQET-inspired form for the m_h -dependence and set η_A to 1, resulting in the first line of our fit form, Eq. (20). This is sufficient to test, through the results we obtain for l_A , l_V and l_P using this expression, that the HQET expectation for the approximate size of these coefficients is fulfilled. We take priors on $l_{A,V,P}$ in our fit of $0 \pm 1 \text{ GeV}^2$.

We have several different proxies, derived from heavy meson masses, that we can take for the heavy quark mass that appears in ε_h in Eq. (20). We do not expect our physical result for $h_{A_1}^s$ to vary significantly depending on which meson mass we use, but the results for l_A , l_V and l_P will vary because of different sub-leading terms in the relationship between meson and quark mass. The most obvious substitutions to use for the heavy quark mass are the mass of the pseudoscalar heavy-strange meson, M_{H_s} , and half the mass of the pseudoscalar heavyonium meson, M_{η_h} . We also tested using the quark mass in the minimal renormalon subtracted (MRS) scheme suggested in [95]. This takes

$$m_h = M_{H_s} - \bar{\Lambda}_{\text{MRS}} - \frac{\mu_{\text{MRS}}^2}{M_{H_s} - \bar{\Lambda}_{\text{MRS}}} + \mathcal{O}\left(\frac{1}{m_h^2}\right). \quad (23)$$

where $\mu_{\text{MRS}}^2 = \mu_{\pi,\text{MRS}}^2 - d_{H^{(*)}} \mu_{G,\text{MRS}}^2$ with $d_{H^{(*)}} = 1$ for pseudoscalar mesons and $-1/3$ for vectors. For this case we use parameters determined in [94] for the MRS scheme: $\bar{\Lambda}_{\text{MRS}} = 0.552(30) \text{ GeV}$, $\mu_{\pi,\text{MRS}}^2 = 0.06(22) \text{ GeV}^2$ and $\mu_{G,\text{MRS}}^2 = 0.38(1) \text{ GeV}^2$. We take m_h from Eq. (23) using our results for the mass of the pseudoscalar heavy-strange meson and m_c from our results for the mass of the D_s^* meson.

We take our central fit, for simplicity, from the result of using half the pseudoscalar heavyonium mass for m_h and half the pseudoscalar charmonium mass for m_c i.e. taking

$$\varepsilon_q \equiv \frac{2}{M_{\eta_q}}. \quad (24)$$

We test the stability of the fit results under the different choices discussed above in Section III B.

2. Mistuning of other quark masses

Our calculation has results for multiple different heavy quark masses on each gluon field configuration. The valence charm and strange quark masses, however, are tuned to their physical values. This is done by fixing the η_c and η_s meson masses to their physical values in a pure QCD world allowing, for example, for η_c annihilation as discussed in [70]. Any possible mistuning of the charm

quark mass is accounted for in our fit function by the dependence on the charm quark mass that is included in the first line of Eq. (20). When the fit function is evaluated at the physical point we set ε_c from the physical η_c mass.

The strange (valence and sea) and light (sea) mass mistunings are accounted for using the tuning in [70]. For the strange quark, we define $\delta_s = m_s - m_s^{\text{tuned}}$, where m_s^{tuned} is given by

$$m_s^{\text{tuned}} = m_{s0} \left(\frac{M_{\eta_s}^{\text{physical}}}{M_{\eta_s}} \right)^2. \quad (25)$$

$M_{\eta_s}^{\text{physical}}$ is determined in lattice simulations from the masses of the pion and kaon [82]. The ratio $\delta_s/m_s^{\text{tuned}}$ then gives the fractional mistuning. The valence strange quark masses are very well tuned, but the sea strange quark masses less so.

We similarly account for mistuning of the masses of the (sea) light quarks by defining $\delta_l = m_l - m_l^{\text{tuned}}$. We find m_l^{tuned} from m_s^{tuned} , leveraging the fact that the ratio of quark masses is regularization independent, and the ratio was calculated in [71]:

$$\left. \frac{m_s}{m_l} \right|_{\text{phys}} = 27.18(10). \quad (26)$$

We set m_l^{tuned} to m_s^{tuned} divided by this ratio.

The full term we include to account for mistuning is then given by

$$\mathcal{N}_{\text{mistuning}} = \frac{c_s^{\text{val}} \delta_s^{\text{val}} + c_s \delta_s + 2c_l \delta_l}{10m_s^{\text{tuned}}} \quad (27)$$

where c_l , c_s and c_s^{val} are fit parameters with prior distributions 0 ± 1 . We neglect $\delta_{s,l}^2$ contributions since these are an order of magnitude smaller and are not resolved in the results of our lattice calculation.

The gluon field configurations that we use have $m_u = m_d \equiv m_l$ in the sea. In the real world this is not true. We test the impact of possible isospin-breaking on our fits by testing for sensitivity to the sea light quark masses. We do this by changing the m_l^{tuned} value up and down by the expected value for $m_d - m_u$ [46]. We find the effect to be completely negligible in comparison to the other sources of error.

3. Discretisation Effects

Discretisation effects in our lattice QCD results are accounted for following the methodology of [68]. We take

$$\mathcal{N}_{\text{disc}} = \sum_{i=0, j+k \neq 0}^{2,2,2} d_{ijk} \left(\frac{2\Lambda_{\text{QCD}}}{M_{\eta_h}} \right)^i \left(\frac{am_{h0}^{\text{val}}}{\pi} \right)^{2j} \left(\frac{am_{c0}^{\text{val}}}{\pi} \right)^{2k}. \quad (28)$$

The leading terms, with $i = 0$, allow for discretisation effects that are set by the heavy quark mass and also discretisation effects that are set by the charm quark mass (or indeed any other lighter scale that is independent of heavy quark mass). The $i > 0$ terms allow for discretisation effects to vary as the heavy quark mass is varied, with M_{η_h} being used here as a proxy for the heavy quark mass. d_{ijk} are fit parameters with prior distributions 0 ± 1.0 . All discretisation effects are of even order by construction of the HISQ action [59].

We tested the impact on the fit of including extra discretisation effects set by the scale Λ_{QCD} but this made no difference (since such effects are much smaller than those already included by the am_{c0}^{val} terms). We also tested the effects of increasing the number of terms in each sum, but the final result remained unchanged.

4. Finite-volume Effects

The finite volume effects in our lattice results are expected to be negligible, because we are working with heavy mesons that have no valence light quarks and no Zweig-allowed strong decay modes. Coupling to chiral loops or decay channels with pions that could produce significant finite-volume effects [96] is therefore absent and we can safely ignore finite-volume effects here.

In section III B we detail the results of several tests of the stability of our final result under changes to the details of the fit.

5. Topological Charge Effects

It has been observed that the finest MILC ensembles ($a \simeq 0.45\text{fm}$ and finer) suffer from slow variation in the topological charge [97] with Monte Carlo time. The question then arises if physical observables obtained by averaging over the ensemble could be biased by being measured in only a small range of topological charge sectors. This issue is addressed in [97] through a calculation of the ‘topological adjustment’ needed for meson masses and decay constants on the ultrafine lattices used here (with $m_l/m_s = 0.2$). The adjustment found for the D_s decay constant is 0.002%. We might expect the impact of a frozen topological charge on $h_{A_1}^s(1)$ to be of a similar size to this, given that it involves a transition between heavy-strange mesons. Allowing for this systematic uncertainty (or even ten times it) has a negligible effect on our final result.

III. RESULTS AND DISCUSSION

A. Result for $h_{A_1}^s(1)$

The results of our correlation function fits (discussed in Section II C) are given in Table II. We tabulate values

for $h_{A_1}^s(1)$ at each heavy quark mass that we have used on each gluon field ensemble from Table I. We also tabulate the meson masses needed to allow determination of $h_{A_1}^s(1)$ at the physical point, using the fit form of Eq. 20.

The fit function of Eq. (20) is readily applied, giving a $\chi^2/[\text{dof}]$ of 0.21 for 12 degrees of freedom. Figure 2 shows our results for $h_{A_1}^s(1)$ along with the fit function at zero lattice spacing and physical u/d , s and c quark masses as the grey band. Evaluating the fit function at the physical b mass, as determined by M_{η_b} , gives our final result

$$\mathcal{F}^{B_s \rightarrow D_s^*}(1) = h_{A_1}^s(1) = 0.9020(96)_{\text{stat}}(90)_{\text{sys}}. \quad (29)$$

Adding the statistical and systematic errors in quadrature, we find a total fractional error of 1.5%. The error budget for this result is given in table IV. Note that we allow for an additional $\pm 10\text{MeV}$ uncertainty in the physical value of the η_b mass beyond the experimental uncertainty, since our lattice QCD results do not include the effect of η_b annihilation and QED [68]. This has no effect, however, since the heavy quark mass dependence is so mild.

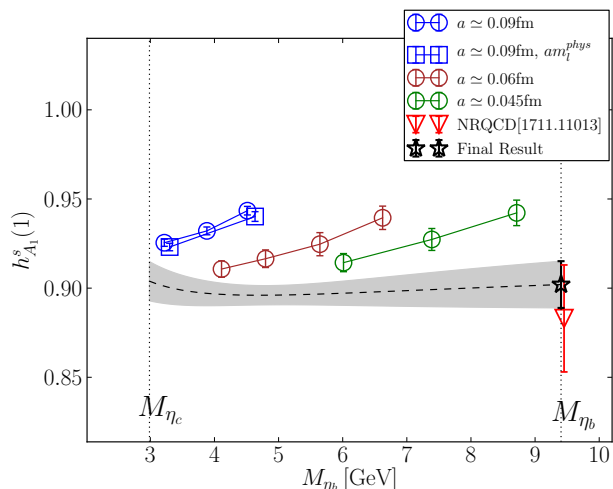


FIG. 2: $h_{A_1}^s(1)$ against M_{η_h} (a proxy for the heavy quark mass). The grey band shows the result of the extrapolation to $a = 0$ at physical l, s and c masses; the black star shows our result at the physical b quark mass. Gluon field ensembles listed in the legend follow the order of sets in Table I. Solid lines simply join the points on a given ensemble for added clarity. The red inverted triangle gives the determination of the same quantity from a previous study using the NRQCD action for the b quark [41].

Our total uncertainty is dominated by the statistical errors in our lattice results. The systematic error is dominated by that from the continuum extrapolation.

We include in Figure 2 the value from the only other lattice determination of $h_{A_1}^s(1)$ [41]. This calculation also used MILC $n_f = 2 + 1 + 1$ gluon field ensembles, but with the bulk of the ensembles used having coarser lattice spacing. This was made possible by the use of the NRQCD action for the b quark [58]. The HISQ action

| Source | % Fractional Error |
|-----------------------|--------------------|
| Statistics + Z_A | 1.06 |
| $a \rightarrow 0$ | 0.73 |
| $m_h \rightarrow m_b$ | 0.69 |
| mass mistuning | 0.20 |
| Total | 1.45 |

TABLE IV: Error budget for $h_{A_1}^s(1)$. Errors are given as a percentage of the final answer. The mass mistuning error includes that from valence strange and sea light and strange quarks; we find that taking a ± 10 MeV uncertainty in the physical value of the η_b mass has a negligible effect.

was used for all the other quarks. The result of this calculation was: $h_{A_1}^s(1) = 0.883(12)_{\text{stat}}(28)_{\text{sys}}$. Our result is in agreement with this, but with substantially smaller errors. The NRQCD uncertainty of 3.4% is dominated by the systematic error from the $\mathcal{O}(\alpha_s)$ matching factor used to normalise the NRQCD-HISQ current and this error is absent from our calculation.

In addition to a value for $h_{A_1}^s(1)$ our calculation is able to give information on the physical dependence on the heavy quark mass of $\mathcal{F}^{H_s \rightarrow D_s^*}(1)$. We see from Figure 2 that this dependence is very mild to the point of being absent. We can determine the ratio of $\mathcal{F}^{H_s \rightarrow D_s^*}(1)$ for $m_h = m_b$ to $m_h = m_c$ (albeit that this latter point corresponds to an unphysical $D_s \rightarrow D_s^*$ decay) and find the value 0.998(23). Each of the terms (including η_A) in the HQET expectation of Eq. 21 can give effects of order a few percent to this ratio. The fact that we find no heavy quark mass dependence at the level of 2% shows that these effects must tend to cancel out.

The fit of our lattice results to Eq. (20) gives fit parameters $l_{V,A,P}^s$ which, as discussed in Section II E 1, provide a test of HQET. We find

$$\begin{aligned} l_V^s &= 0.71(28)\text{GeV}^2, \\ l_A^s &= -0.34(32)\text{GeV}^2, \\ l_P^s &= -0.53(34)\text{GeV}^2, \end{aligned} \quad (30)$$

from our baseline fit. These results are compatible with values of $\mathcal{O}(\Lambda_{\text{QCD}}^2)$ as expected by HQET. As discussed in Section II E 1 these fit parameters change depending on the proxy that we use for the quark mass as well as our treatment of η_A . However, as we show in the tests performed in the next section (see Figure 5) this has little impact on our value for $h_{A_1}^s(1)$.

B. Further tests of our fit

Because we tune our b and c valence quark masses using the pseudoscalar heavyonium meson mass, we can independently test our results by comparing both our heavy-strange and D_s^* meson masses against experiment.

These results are shown in Figures 3 and 4. In each case we subtract half the corresponding pseudoscalar heavyonium mass to reduce lattice spacing uncertainties in the comparison to experiment [87].

Figure 3 shows that our D_s^* meson mass agrees with experiment on all our ensembles at the level of our 5 MeV uncertainties. Systematic effects from missing QED and η_c annihilation are expected to be of size a few MeV [87].

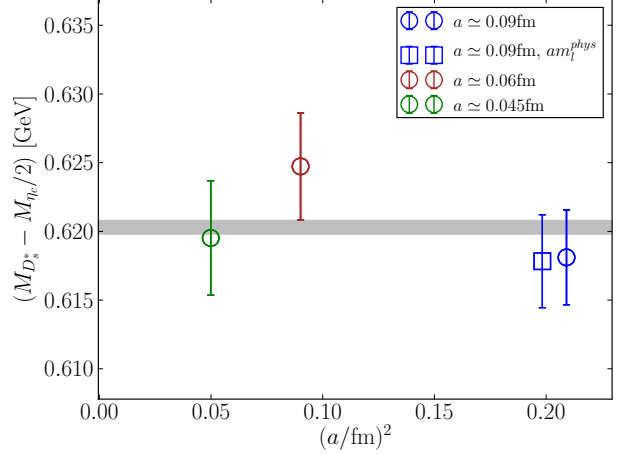


FIG. 3: The D_s^* meson mass obtained on each of our gluon field ensembles, given as a difference from one half the η_c meson mass. Errors include statistical and lattice spacing uncertainties. The grey band gives the experimental result [46].

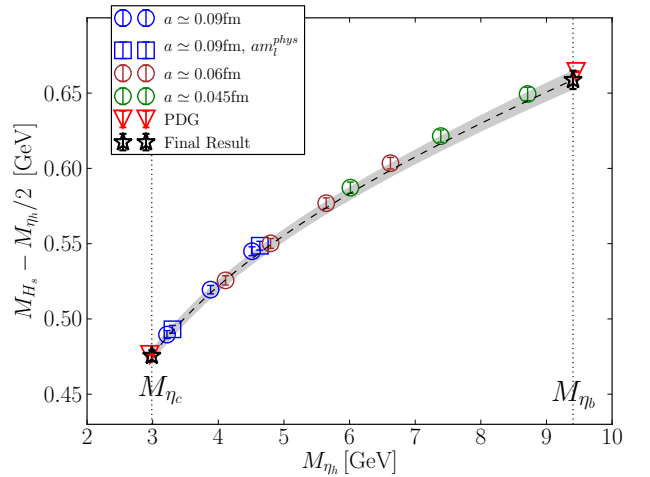


FIG. 4: The H_s meson mass obtained on each of our gluon field ensembles, given as a difference to one half of the η_h meson mass. Errors include statistical and lattice spacing uncertainties. The grey band gives a fit to the heavy-quark mass dependence as discussed in the text, with black stars giving our results at $m_h = m_c$ and $m_h = m_b$. The inverted red triangles give the corresponding experimental values [46].

Figure 4 shows our results for the heavy-strange pseudoscalar meson mass as a function of the pseudoscalar heavyonium mass. We show the difference $\Delta_h = M_{H_s} - M_{\eta_h}/2$ to remove the leading m_h dependence and also to reduce uncertainties from the value of the lattice spacing. We fit Δ_h to a simple function of ε_h (Eq. (24)) :

$$\Delta_h(a, m_l, m_h) = \left(\sum_{i=-1}^{i=1} c_i \varepsilon_h^i \right) \times (1 + \mathcal{N}_{\text{disc}} + \mathcal{N}_{\text{mistuning}}). \quad (31)$$

The leading, linear, term in ε_h allows for the fact that the heavyonium (η_h) binding energy grows linearly with m_h in a $1/r$ potential. We take priors on the c_i of: $c_{-1} : 0.05(5)$; $c_0 : 0.5(5)$; $c_1 : 0(1)$. $\mathcal{N}_{\text{disc}}$ takes the same form as in Eq. (28) with $a\Lambda_{\text{QCD}}$ (where Λ_{QCD} is taken as 0.5 GeV) replacing am_{c0}^{val} , which is not relevant here. $\mathcal{N}_{\text{mistuning}}$ takes the same form as in Eq. (27).

Our result for the difference $M_{H_s} - M_{\eta_h}/2$ in the continuum at $m_h = m_c$ is 0.4755(37) GeV and at $m_h = m_b$ is 0.6588(61) GeV. These agree well with the earlier HPQCD results on $n_f = 2 + 1$ gluon field configurations of 0.4753(22) GeV [87] and 0.658(11) GeV [67]. They also agree well with the experimental values of 0.4764(3) GeV and 0.6674(12) GeV [46], allowing for the ~ 3 –5 MeV effect from missing QED and η_b and η_c annihilation processes in the lattice QCD results.

We also performed a number of tests of our continuum/heavy-quark mass dependence fit to our results for $h_{A_1}^s(1)$. These are tabulated graphically in Figure 5.

One of the tests, denoted ‘Ratio with f_{H_c} ’ in Figure 5, is described in more detail in Appendix A. It involves fitting the ratio of $h_{A_1}^s(1)$ to the H_c decay constant, as a function of heavy quark mass and, after determining the continuum result at $m_h = m_b$, multiplying by the value for the B_c decay constant determined from lattice QCD to obtain $h_{A_1}^s(1)$. The reason for doing this is because this ratio has smaller discretisation effects than $h_{A_1}^s(1)$ alone, as is clear from Figure 8 in Appendix A. It has stronger dependence on m_h , however, coming from the H_c decay constant, along with sizeable uncertainties introduced from the uncertainty in the lattice spacing. Another disadvantage is that the physical result for H_c decay constant must also be obtained. We find that this method gives results in agreement with our standard fit but with significantly larger uncertainties. It provides a good test, however, because it has very different m_h dependence.

C. Implications for $B \rightarrow D^*$

As discussed in Section I, $h_{A_1}^s(1)$ is expected to be close in value to the equivalent $B \rightarrow D^*$ form factor, since they only differ in the mass of the light spectator quark and in effects arising from the strong decay of the D^* to $D\pi$. In [41] the ratio of the two form factors was

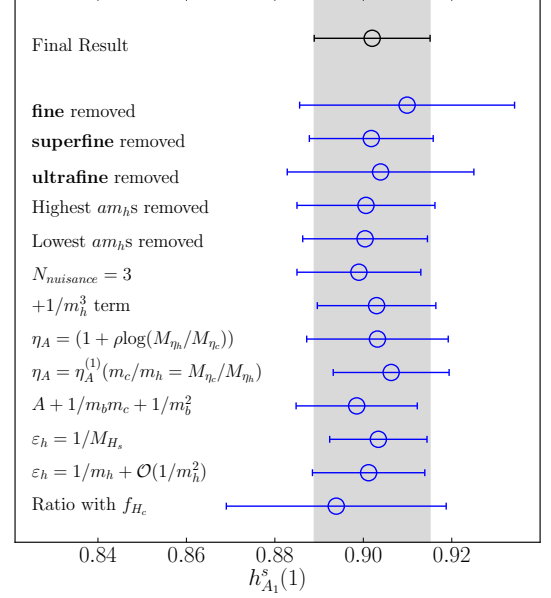


FIG. 5: Results of testing the fit to $h_{A_1}^s(1)$ results. The top black point gives our baseline fit result in the continuum and at physical b quark mass. The top three blue points show the corresponding value if results from the fine, superfine or ultrafine ensembles are dropped from the fit. The fourth and fifth blue points show the result if instead results at the highest/lowest am_{h0}^{val} value on each ensemble are removed. ‘ $N_{\text{nuisance}} = 3$ ’ shows the result of truncating each sum in $\mathcal{N}_{\text{disc}}$ (28) at 3 rather than 2. ‘ $+1/m_b^3$ ’ results from adding an extra term to (20) of the form $p/M_{\eta_h}^3$ where p is a fit parameter with the same prior as $l_{V,A,P}^2$. In this case the Bayes factor falls by a factor of 7, suggesting that the results do not contain a cubic dependence on the heavy mass. The next two points show the results of including specific implementations of η_A described in Section II E (rather than the value 1). In the upper variant parameter ρ is given prior 0 ± 1 . The lower variant shows the result of using the 1-loop expression for η_A (Eq. (22)), with m_c/m_h replaced with M_{η_c}/M_{η_h} . ‘ $A + 1/m_b m_c + 1/m_b^2$ ’ is the result of replacing $1 + l_V/m_c^2$ in the fit with a fit parameter A with prior distribution 1 ± 1 . The fact that this does not affect the fit shows that mistuning of the charm quark mass is a negligible effect here. The points with labels beginning ‘ $\varepsilon_h =$ ’ show the result of replacing the heavy mass proxy $M_{\eta_h}/2$ with M_{H_s} and the MRS quark mass (Eq. (23)) respectively. The bottom point labelled ‘Ratio with f_{H_c} ’ is the result of an alternative extrapolation described in Appendix A.

found to be: $h_{A_1}(1)/h_{A_1}^s(1) = 1.013(14)_{\text{stat}}(17)_{\text{sys}}$. Note that systematic effects from the perturbative matching of the NRQCD-HISQ current largely cancel in this ratio.

Multiplying this by our result for $h_{A_1}^s(1)$, we can determine $h_{A_1}(1)$ as

$$\mathcal{F}^{B \rightarrow D^*}(1) = h_{A_1}(1) = 0.914(24) \quad (32)$$

adding all the uncertainties in quadrature.

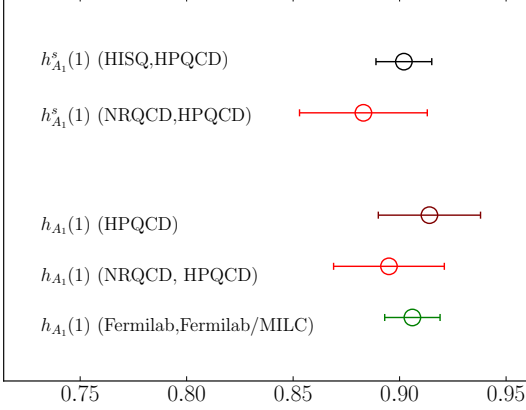


FIG. 6: Comparison of lattice QCD results for $h_{A_1}^s(1)$ and $h_{A_1}(1)$. Our results for $h_{A_1}^s(1)$ are marked ‘(HISQ, HPQCD)’ and for $h_{A_1}(1)$ are marked ‘(HPQCD)’. Those marked ‘(NRQCD, HPQCD)’ are from [41] and the value marked ‘(Fermilab, Fermilab/MILC)’ is from [39].

In Figures 6 and 7, we compare current lattice results for $h_{A_1}(1)$ and $h_{A_1}^s(1)$. Figure 6 compares final results for $h_{A_1}^s(1)$ from the HPQCD calculation using NRQCD b quarks and HISQ lighter quarks [41] with our full HISQ result given here (Eq. (29)). It also compares final results for $h_{A_1}(1)$ from using the Fermilab approach [39] for b and c quarks and asqtad light quarks, NRQCD b quarks and HISQ lighter quarks [41] and our result from Eq. 32 using the strange to light ratio from [41]. Good agreement between all results is seen, well within the uncertainties quoted.

In Figure 7, we show more detail of the comparison by plotting the lattice results from the previous Fermilab/MILC [39] and NRQCD b [41] calculations as a function of the valence spectator light quark mass (given by the square of the pion mass). Note that, for the results for $h_{A_1}(1)$ to the left of the plot, the valence light and sea masses are the same. For the $h_{A_1}^s(1)$ points from [41] to the right of the plot, the sea light (along with s and c) quark masses take their physical values. Although agreement for $h_{A_1}(1)$ is seen at physical light quark mass in the continuum limit from all approaches, the NRQCD-HISQ results show systematic light quark mass dependence away from this point that is not visible in the Fermilab/MILC results. The two sets of results move apart as the spectator quark mass increases, and it is therefore not clear how well they would agree for spectator s quarks.

Our results, shown in Figure 7 with black stars, agree with the NRQCD-HISQ results for $h_{A_1}^s(1)$. The smaller uncertainties from using a fully nonperturbative current normalisation here show that the perturbative matching uncertainty allowed for in [41] was conservative. Using the s/l ratio from this calculation, where the perturba-

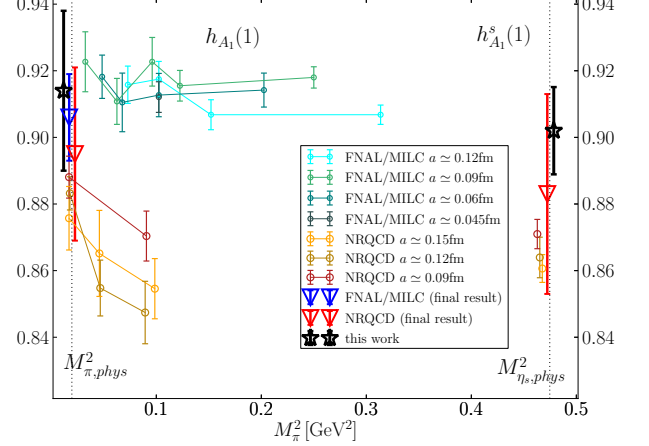


FIG. 7: More detailed comparison of lattice QCD results for $h_{A_1}(1)$ (left side) and $h_{A_1}^s(1)$ (right side). Raw results for $h_{A_1}(1)$ are from [41] and [39] and are plotted as a function of valence (=sea) light quark mass, given by the square of M_π . On the right are points for $h_{A_1}^s(1)$ from [41] plotted at the appropriate valence mass for the s quark, but obtained at physical sea light quark masses. The final result for $h_{A_1}(1)$ from [39], with its full error bar, is given by the inverted blue triangle. The inverted red triangles give the final results for $h_{A_1}(1)$ and $h_{A_1}^s(1)$ from [41]. Our results here are given by the black stars.

tive matching uncertainty cancels, allows us to obtain an $h_{A_1}(1)$ result that agrees well with both earlier values. Our uncertainty on $h_{A_1}(1)$ is similar to that from [41] once we have combined the uncertainty from the ratio with that from our value for $h_{A_1}^s(1)$. However we have removed the perturbative matching uncertainty that dominates the NRQCD-HISQ error.

IV. CONCLUSIONS

We have calculated the form factor at zero recoil, $\mathcal{F}^{B_s \rightarrow D_s^*}(1)$ or $h_{A_1}^s(1)$, using the relativistic HISQ formalism in full lattice QCD. This allows us to normalise the $b \rightarrow c$ current fully nonperturbatively for the first time and to determine how the form factor depends on the heavy quark mass (at physical charm quark mass). Our results show that dependence on the heavy quark mass is very mild (see Figure 2).

Our result

$$\mathcal{F}^{B_s \rightarrow D_s^*}(1) = h_{A_1}^s(1) = 0.9020(96)_{\text{stat}}(90)_{\text{sys}} \quad (33)$$

agrees with an earlier lattice QCD result [41], but with half the uncertainty because of the nonperturbative normalisation of the current. Using the strange to light quark ratio from the earlier paper we are able to obtain a result for $\mathcal{F}^{B \rightarrow D^*}(1)$

$$\mathcal{F}^{B \rightarrow D^*}(1) = h_{A_1}(1) = 0.914(24) \quad (34)$$

which is also free of perturbative matching uncertainties.

$h_{A_1}^s(1)$ will be a useful value to compare to experimental results in future to determine V_{cb} . It has some advantages from a lattice QCD perspective over h_{A_1} as discussed in Section I. However, $h_{A_1}(1)$ can be combined with existing experimental results to obtain a value for the CKM element V_{cb} . The method of combination has been questioned recently when it was realised that the HQET constraints on the extrapolation of the exclusive experimental data to the zero recoil point were having a significant effect. Loosening these constraints gives a higher, but less precise, value for the combination $|\bar{\eta}_{EW} V_{cb}| h_{A_1}(1)$ (see, for example, the V_{ub}/V_{cb} mini-review in [46]). Combining this experimental value with lattice QCD results for $h_{A_1}(1)$ then gives a result for V_{cb} from the $B \rightarrow D^* \ell \nu$ exclusive decay that agrees with, but is less accurate than, that from inclusive $b \rightarrow c$ decays. We do not convert our h_{A_1} result into a value for V_{cb} here since it is clear from Figure 6 that we will agree with existing results (such as that in [41]) and, on its own, our new result does not have sufficient accuracy to reduce uncertainties in V_{cb} .

In future lattice QCD form factor calculations for both $B_s \rightarrow D_s^*$ and $B \rightarrow D^*$ need to work away from zero recoil to improve overlap with experimental results without the need for extrapolation¹. Our results here demonstrate the efficacy of HPQCD’s ‘heavy HISQ’ approach for form factors at zero recoil. Away from zero recoil we expect it to be even more useful because it is possible to map out the full q^2 range of the decay [73], where non-relativistic approaches must stay close to zero recoil because of systematic errors that grow with the magnitude of the daughter meson momentum. Heavy HISQ calculations are underway for the form factors for $B_{(s)} \rightarrow D_{(s)}^*$, $B_c \rightarrow J/\psi$ decay, and the related $B_s \rightarrow D_s$ decay over the full q^2 range, using the techniques developed for $c \rightarrow s$ decays to normalise the currents nonperturbatively [51, 84]. Initial results [74, 99] look very promising.

Acknowledgements

We are grateful to the MILC collaboration for the use of their configurations and their code. Computing was done on the Cambridge Service for Data Driven Discovery (CSD3) supercomputer, part of which is operated by the University of Cambridge Research Computing Service on behalf of the UK Science and Technology Facilities Council (STFC) DiRAC HPC Facility. The DiRAC component of CSD3 was funded by BEIS via STFC capital grants and is operated by STFC operations grants.

¹ Preliminary results using the Fermilab formalism for b and c quarks and asqtad light quarks have already appeared [98], as have results using Möbius domain-wall quarks with a range of m_h values up to $2.44m_c$ [62].

We are grateful to the CSD3 support staff for assistance. Funding for this work came from STFC. We would also like to thank C. Bouchard, B. Colquhoun, D. Hatton, J. Harrison, P. Lepage and M. Wingate for useful discussions.

APPENDIX A: RATIO METHOD FOR DETERMINING $h_{A_1}^s(1)$

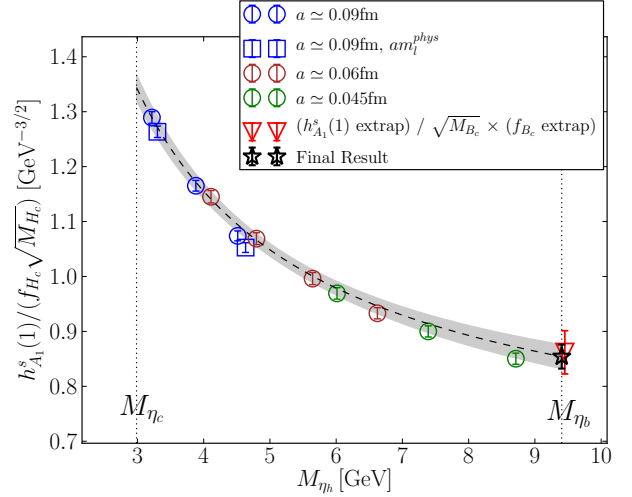


FIG. 8: The ratio $h_{A_1}^s(1)/(f_{H_c} \sqrt{M_{H_c}})$ plotted against M_{η_h} (a proxy for the heavy quark mass). Gluon field ensembles listed in the legend follow the order of sets in Table I. The grey band shows the result of the fit described in the text, evaluated at $a = 0$ and physical l , s and c quark masses to give the physical heavy quark mass dependence of the ratio. At $m_h = m_b$ we obtain the result given by the black star. For comparison with our previous fit for $h_{A_1}^s(1)$ the inverted red triangle shows our result from Eq. (33) converted to a ratio using the value for f_{B_c} from Figure 9 and M_{B_c} from experiment [46].

It turns out that the significant discretisation effects visible in our results for $h_{A_1}^s(1)$ (Figure 2) are largely cancelled when we divide them by lattice QCD results for the decay constant of the heavy-charm pseudoscalar meson, f_{H_c} . This was also observed in [74] for vector form factors involving a $b\bar{c}$ current. f_{H_c} is determined from the matrix element between the vacuum and the H_c meson of the temporal axial vector $b\bar{c}$ current, whereas $h_{A_1}^s(1)$ is the matrix element between the H_s and D_s^* mesons of the spatial axial vector $b\bar{c}$ current. They behave very differently as a function of heavy quark mass but in practice have similar discretisation errors (compare Figures 2 and 9). We can make use of this in fitting the heavy quark mass dependence of their ratio with reduced discretisation effects. We also then need to fit the H_c decay constant on its own in order to determine a physical value for the B_c that we can use to determine $h_{A_1}^s(1)$ at the physical point.

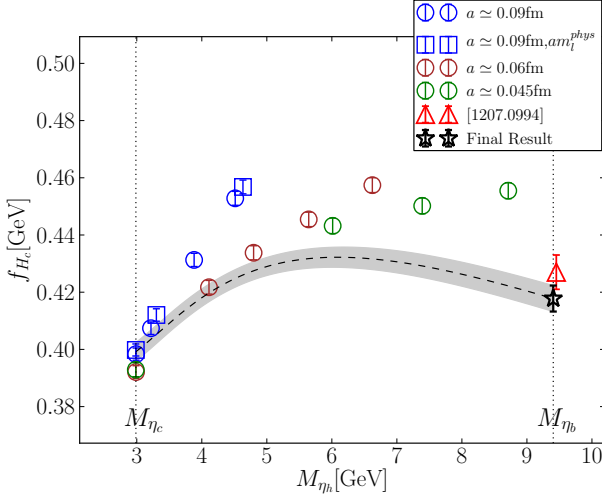


FIG. 9: The heavy-charm pseudoscalar meson decay constant, f_{H_c} , plotted against M_{η_h} (a proxy for the heavy quark mass). Gluon field ensembles listed in the legend follow the order of sets in Table I. The grey band shows the result of the fit described in the text, evaluated at $a = 0$ and physical l , s and c quark masses to give the physical heavy quark mass dependence of the decay constant. At $m_h = m_b$ we obtain the result given by the black star. The red triangle shows the result from a previous heavy HISQ determination of f_{B_c} on $n_f = 2 + 1$ gluon field ensembles [68].

f_{H_c} is found using the PCAC relation for HISQ quarks

$$f_{H_c} = \frac{m_{h0} + m_{c0}}{M_{H_c}^2} \langle 0 | P | H_c \rangle |_{\text{lat}}, \quad (\text{A1})$$

where $\langle 0 | P | H_c \rangle$ is determined in the fit to the H_c two-point correlation functions via (14). We use a pseudoscalar operator, P , with spin-taste $\gamma_5 \otimes \gamma_5$ so f_{H_c} is absolutely normalised. Results for f_{H_c} for each ensemble are given in Table II and plotted in Figure 9.

On each ensemble, at each heavy quark mass, we form the ratio $h_{A_1}^s(1)/(f_{H_c}\sqrt{M_{H_c}})$, plotted in Figure 8. Although discretisation effects largely cancel, the ratio varies strongly with changing heavy quark mass. This makes fitting this ratio as a function of heavy quark mass and lattice spacing very different to that of $h_{A_1}^s(1)$, with different systematic effects.

We use a fit function of the same form for both $h_{A_1}^s(1)/(f_{H_c}\sqrt{M_{H_c}})$ and f_{H_c} . Denoting the quantity being fit by F , we write (following [68]):

$$F(a, m_h, m_l) = A \left(\frac{\alpha_s(M_{\eta_h}/2)}{\alpha_s(M_{\eta_c}/2)} \right)^p M_{\eta_h}^{n/2} \times \quad (\text{A2})$$

$$\sum_{i,j,k=0}^{2,2,2} d_{ijk} \left(\frac{2 \text{ GeV}}{M_{\eta_h}} \right)^i \left(\frac{am_{h0}^{\text{val}}}{\pi} \right)^{2j} \left(\frac{am_{c0}^{\text{val}}}{\pi} \right)^{2k} \times$$

$$\left(1 + \mathcal{N}_{\text{mistuning}} + c_c \frac{M_{\eta_c} - M_{\eta_c}^{\text{physical}}}{M_{\eta_c}^{\text{physical}}} \right).$$

$\alpha_s(M)$ is the QCD coupling constant evaluated at scale M and the ratio of α_s factors resums leading logarithms in HQET in the decay constant [100]. We take α_s in the $\overline{\text{MS}}$ scheme from lattice QCD [70]. The power p is then $-6/25$ (for $n_f = 4$) for the f_{H_c} fit and $+6/25$ for the fit to the ratio $h_{A_1}^s(1)/(f_{H_c}\sqrt{M_{H_c}})$. The leading power of M_{η_h} , n , is -1 for the fit to f_{H_c} based on HQET expectations, but 0 for the fit to the ratio because we have used $f_{H_c}\sqrt{M_{H_c}}$ in the denominator to remove half-integer powers of ε_h from the fit. The remainder of the fit function allows for inverse powers of m_h and discretisation effects. $\mathcal{N}_{\text{mistuning}}$ is the same as that defined earlier for our $h_{A_1}^s$ fit and is given in Eq. (27). The final term allows for c quark mistuning with prior on c_c of 0 ± 1 . We take a prior on the overall constant A of $0 \pm 4(\text{GeV}^{3/2})$ in the f_{H_c} fit and $0 \pm 2(\text{GeV}^{-3/2})$ in the ratio fit. Priors on the d_{ijk} are taken as 0 ± 2 except for d_{000} which is defined to have value 1.0.

The fit to the ratio is shown in Figure 8 and the fit to f_{H_c} in Figure 9. For the ratio fit χ^2/dof is 0.27 for 12 degrees of freedom and for the f_{H_c} fit, 0.53 for 16. Our final result for f_{H_c} at $m_h = m_b$ agrees with a previous HPQCD heavy HISQ determination on gluon field configurations including $n_f = 2 + 1$ flavours of sea quarks [68] (shown as the red triangle in Figure 9). Our final result for the ratio $h_{A_1}^s(1)/(f_{H_c}\sqrt{M_{H_c}})$ at $m_h = m_b$ can then be multiplied by our value for f_{B_c} and the square root of the mass of the B_c meson from the Particle Data Tables [46], to give $h_{A_1}^s(1)$. This value is shown as the bottom point in Figure 5. Figure 8 compares the result from the ratio fit given by the grey band to the value (shown by inverted red triangle) obtained by taking our baseline fit result for $h_{A_1}^s(1)$ from Eq. (33) and calculating from it the value of the ratio $h_{A_1}^s(1)/(f_{H_c}\sqrt{M_{H_c}})$ using our value for f_{B_c} and the experimental M_{B_c} . The agreement is good, showing the consistency of the two different approaches.

-
- [1] J. T. Wei *et al.* (Belle), *Phys. Rev. Lett.* **103**, 171801 (2009), [arXiv:0904.0770 \[hep-ex\]](#) .
- [2] J. P. Lees *et al.* (BaBar), *Phys. Rev. Lett.* **109**, 101802 (2012), [arXiv:1205.5442 \[hep-ex\]](#) .
- [3] J. P. Lees *et al.* (BaBar), *Phys. Rev.* **D86**, 032012 (2012), [arXiv:1204.3933 \[hep-ex\]](#) .
- [4] J. P. Lees *et al.* (BaBar), *Phys. Rev.* **D88**, 072012 (2013), [arXiv:1303.0571 \[hep-ex\]](#) .
- [5] R. Aaij *et al.* (LHCb), *JHEP* **06**, 133 (2014), [arXiv:1403.8044 \[hep-ex\]](#) .
- [6] R. Aaij *et al.* (LHCb), *Phys. Rev. Lett.* **113**, 151601 (2014), [arXiv:1406.6482 \[hep-ex\]](#) .
- [7] M. Huschle *et al.* (Belle), *Phys. Rev.* **D92**, 072014 (2015), [arXiv:1507.03233 \[hep-ex\]](#) .
- [8] R. Aaij *et al.* (LHCb), *JHEP* **02**, 104 (2016), [arXiv:1512.04442 \[hep-ex\]](#) .
- [9] R. Aaij *et al.* (LHCb), *Phys. Rev. Lett.* **115**, 111803 (2015), [Erratum: *Phys. Rev. Lett.* 115, 159901 (2015)], [arXiv:1506.08614 \[hep-ex\]](#) .
- [10] R. Aaij *et al.* (LHCb), *JHEP* **06**, 115 (2015), [Erratum: *JHEP* 09, 145 (2018)], [arXiv:1503.07138 \[hep-ex\]](#) .
- [11] R. Aaij *et al.* (LHCb), *JHEP* **11**, 047 (2016), [Erratum: *JHEP* 04, 142 (2017)], [arXiv:1606.04731 \[hep-ex\]](#) .
- [12] S. Wehle *et al.* (Belle), *Phys. Rev. Lett.* **118**, 111801 (2017), [arXiv:1612.05014 \[hep-ex\]](#) .
- [13] Y. Sato *et al.* (Belle), *Phys. Rev.* **D94**, 072007 (2016), [arXiv:1607.07923 \[hep-ex\]](#) .
- [14] S. Hirose *et al.* (Belle), *Phys. Rev.* **D97**, 012004 (2018), [arXiv:1709.00129 \[hep-ex\]](#) .
- [15] R. Aaij *et al.* (LHCb), *Phys. Rev.* **D97**, 072013 (2018), [arXiv:1711.02505 \[hep-ex\]](#) .
- [16] R. Aaij *et al.* (LHCb), *Phys. Rev. Lett.* **120**, 171802 (2018), [arXiv:1708.08856 \[hep-ex\]](#) .
- [17] R. Aaij *et al.* (LHCb), *JHEP* **08**, 055 (2017), [arXiv:1705.05802 \[hep-ex\]](#) .
- [18] A. M. Sirunyan *et al.* (CMS), *Phys. Lett.* **B781**, 517 (2018), [arXiv:1710.02846 \[hep-ex\]](#) .
- [19] M. Aaboud *et al.* (ATLAS), *JHEP* **10**, 047 (2018), [arXiv:1805.04000 \[hep-ex\]](#) .
- [20] Y. Amhis *et al.* (HFLAV), *Eur. Phys. J.* **C77**, 895 (2017), [arXiv:1612.07233 \[hep-ex\]](#) .
- [21] A. J. Bevan *et al.* (BaBar, Belle), *Eur. Phys. J.* **C74**, 3026 (2014), [arXiv:1406.6311 \[hep-ex\]](#) .
- [22] A. Alberti, P. Gambino, K. J. Healey, and S. Nandi, *Phys. Rev. Lett.* **114**, 061802 (2015), [arXiv:1411.6560 \[hep-ph\]](#) .
- [23] H. Schroder, in *Heavy quark physics. Proceedings, 138th WE-Heraeus Seminar, Bad Honnef, Germany, December 14-16, 1994* (1994) pp. 9–22.
- [24] D. Bortoletto *et al.* (CLEO), *Phys. Rev. Lett.* **64**, 2117 (1990).
- [25] R. Fulton *et al.* (CLEO), *Phys. Rev.* **D43**, 651 (1991).
- [26] H. Albrecht *et al.* (ARGUS), *Phys. Lett.* **B275**, 195 (1992).
- [27] B. Barish *et al.* (CLEO), *Phys. Rev.* **D51**, 1014 (1995), [arXiv:hep-ex/9406005 \[hep-ex\]](#) .
- [28] D. Buskulic *et al.* (ALEPH), *Phys. Lett.* **B384**, 449 (1996).
- [29] D. Buskulic *et al.* (ALEPH), *Nucl. Instrum. Meth.* **A346**, 461 (1994).
- [30] G. Abbiendi *et al.* (OPAL), *Phys. Lett.* **B482**, 15 (2000), [arXiv:hep-ex/0003013 \[hep-ex\]](#) .
- [31] P. Abreu *et al.* (DELPHI), *Phys. Lett.* **B510**, 55 (2001), [arXiv:hep-ex/0104026 \[hep-ex\]](#) .
- [32] N. E. Adam *et al.* (CLEO), *Phys. Rev.* **D67**, 032001 (2003), [arXiv:hep-ex/0210040 \[hep-ex\]](#) .
- [33] J. Abdallah *et al.* (DELPHI), *Eur. Phys. J.* **C33**, 213 (2004), [arXiv:hep-ex/0401023 \[hep-ex\]](#) .
- [34] B. Aubert *et al.* (BaBar), *Phys. Rev.* **D77**, 032002 (2008), [arXiv:0705.4008 \[hep-ex\]](#) .
- [35] B. Aubert *et al.* (BaBar), *Phys. Rev. Lett.* **100**, 231803 (2008), [arXiv:0712.3493 \[hep-ex\]](#) .
- [36] B. Aubert *et al.* (BaBar), *Phys. Rev.* **D79**, 012002 (2009), [arXiv:0809.0828 \[hep-ex\]](#) .
- [37] W. Dungen *et al.* (Belle), *Phys. Rev.* **D82**, 112007 (2010), [arXiv:1010.5620 \[hep-ex\]](#) .
- [38] A. Abdesselam *et al.* (Belle), (2017), [arXiv:1702.01521 \[hep-ex\]](#) .
- [39] J. A. Bailey *et al.* (Fermilab Lattice, MILC), *Phys. Rev.* **D89**, 114504 (2014), [arXiv:1403.0635 \[hep-lat\]](#) .
- [40] A. Abdesselam *et al.* (Belle), (2018), [arXiv:1809.03290 \[hep-ex\]](#) .
- [41] J. Harrison, C. Davies, and M. Wingate (HPQCD), *Phys. Rev.* **D97**, 054502 (2018), [arXiv:1711.11013 \[hep-lat\]](#) .
- [42] J. A. Bailey, S. Lee, W. Lee, J. Leem, and S. Park, *Phys. Rev.* **D98**, 094505 (2018), [arXiv:1808.09657 \[hep-lat\]](#) .
- [43] F. U. Bernlochner, Z. Ligeti, M. Papucci, and D. J. Robinson, *Phys. Rev.* **D95**, 115008 (2017), [Erratum: *Phys. Rev.* D97, no. 5, 059902 (2018)], [arXiv:1703.05330 \[hep-ph\]](#) .
- [44] D. Bigi, P. Gambino, and S. Schacht, *Phys. Lett.* **B769**, 441 (2017), [arXiv:1703.06124 \[hep-ph\]](#) .
- [45] B. Grinstein and A. Kobach, *Phys. Lett.* **B771**, 359 (2017), [arXiv:1703.08170 \[hep-ph\]](#) .
- [46] M. Tanabashi *et al.* (Particle Data Group), *Phys. Rev.* **D98**, 030001 (2018).
- [47] J. P. Lees *et al.* (BaBar), (2019), [arXiv:1903.10002 \[hep-ex\]](#) .
- [48] G. Caria (Belle), “Measurement of $R(D)$ and $R(D^*)$ with a Semileptonic tag at Belle,” (2019), 54th Rencontres de Moriond on Electroweak Interactions, March 16–23, 2019, La Thuile, Italy.
- [49] G. C. Donald, C. T. H. Davies, J. Koponen, and G. P. Lepage (HPQCD), *Phys. Rev. Lett.* **112**, 212002 (2014), [arXiv:1312.5264 \[hep-lat\]](#) .
- [50] J. A. Bailey *et al.* (Fermilab/MILC), *Phys. Rev.* **D85**, 114502 (2012), [Erratum: *Phys. Rev.* D86, 039904 (2012)], [arXiv:1202.6346 \[hep-lat\]](#) .
- [51] J. Koponen, C. T. H. Davies, G. C. Donald, E. Follana, G. P. Lepage, H. Na, and J. Shigemitsu (HPQCD), (2013), [arXiv:1305.1462 \[hep-lat\]](#) .
- [52] C. J. Monahan, H. Na, C. M. Bouchard, G. P. Lepage, and J. Shigemitsu (HPQCD), *Phys. Rev.* **D95**, 114506 (2017), [arXiv:1703.09728 \[hep-lat\]](#) .
- [53] E. E. Jenkins and M. J. Savage, *Phys. Lett.* **B281**, 331 (1992).
- [54] C. Bernard *et al.* (Fermilab/MILC), *Phys. Rev.* **D79**, 014506 (2009), [arXiv:0808.2519 \[hep-lat\]](#) .
- [55] A. X. El-Khadra, A. S. Kronfeld, and P. B. Mackenzie,

- Phys. Rev. **D55**, 3933 (1997), [arXiv:hep-lat/9604004 \[hep-lat\]](#) .
- [56] A. Bazavov *et al.* (MILC), *Rev. Mod. Phys.* **82**, 1349 (2010), [arXiv:0903.3598 \[hep-lat\]](#) .
- [57] G. P. Lepage, L. Magnea, C. Nakhleh, U. Magnea, and K. Hornbostel, *Phys. Rev.* **D46**, 4052 (1992), [arXiv:hep-lat/9205007 \[hep-lat\]](#) .
- [58] R. J. Dowdall *et al.* (HPQCD), *Phys. Rev.* **D85**, 054509 (2012), [arXiv:1110.6887 \[hep-lat\]](#) .
- [59] E. Follana, Q. Mason, C. Davies, K. Hornbostel, G. P. Lepage, J. Shigemitsu, H. Trotter, and K. Wong (HPQCD, UKQCD), *Phys. Rev.* **D75**, 054502 (2007), [arXiv:hep-lat/0610092 \[hep-lat\]](#) .
- [60] J. Flynn, T. Izubuchi, A. Juttner, T. Kawanai, C. Lehner, E. Lizarazo, A. Soni, J. T. Tsang, and O. Witzel, *PoS LATTICE2016*, 296 (2016), [arXiv:1612.05112 \[hep-lat\]](#) .
- [61] J. A. Bailey, T. Bhattacharya, R. Gupta, Y.-C. Jang, W. Lee, J. Leem, S. Park, and B. Yoon (LANL-SWME), *EPJ Web Conf.* **175**, 13012 (2018), [arXiv:1711.01786 \[hep-lat\]](#) .
- [62] T. Kaneko, Y. Aoki, B. Colquhoun, H. Fukaya, and S. Hashimoto (JLQCD), in *36th International Symposium on Lattice Field Theory (Lattice 2018) East Lansing, MI, United States, July 22-28, 2018* (2018) [arXiv:1811.00794 \[hep-lat\]](#) .
- [63] J. Harada, S. Hashimoto, A. S. Kronfeld, and T. Onogi, *Phys. Rev.* **D65**, 094514 (2002), [arXiv:hep-lat/0112045 \[hep-lat\]](#) .
- [64] C. Monahan, J. Shigemitsu, and R. Horgan, *Phys. Rev.* **D87**, 034017 (2013), [arXiv:1211.6966 \[hep-lat\]](#) .
- [65] A. Bazavov *et al.* (MILC), *Phys. Rev.* **D82**, 074501 (2010), [arXiv:1004.0342 \[hep-lat\]](#) .
- [66] A. Bazavov *et al.* (MILC), *Phys. Rev.* **D87**, 054505 (2013), [arXiv:1212.4768 \[hep-lat\]](#) .
- [67] C. McNeile, C. T. H. Davies, E. Follana, K. Hornbostel, and G. P. Lepage (HPQCD), *Phys. Rev.* **D85**, 031503 (2012), [arXiv:1110.4510 \[hep-lat\]](#) .
- [68] C. McNeile, C. T. H. Davies, E. Follana, K. Hornbostel, and G. P. Lepage, *Phys. Rev.* **D86**, 074503 (2012), [arXiv:1207.0994 \[hep-lat\]](#) .
- [69] C. McNeile, C. T. H. Davies, E. Follana, K. Hornbostel, and G. P. Lepage, *Phys. Rev.* **D82**, 034512 (2010), [arXiv:1004.4285 \[hep-lat\]](#) .
- [70] B. Chakraborty, C. T. H. Davies, B. Galloway, P. Knecht, J. Koponen, G. C. Donald, R. J. Dowdall, G. P. Lepage, and C. McNeile (HPQCD), *Phys. Rev.* **D91**, 054508 (2015), [arXiv:1408.4169 \[hep-lat\]](#) .
- [71] A. Bazavov *et al.* (Fermilab/MILC), *Phys. Rev.* **D98**, 074512 (2018), [arXiv:1712.09262 \[hep-lat\]](#) .
- [72] P. Petreczky and J. H. Weber, (2019), [arXiv:1901.06424 \[hep-lat\]](#) .
- [73] A. Lytle, B. Colquhoun, C. Davies, J. Koponen, and C. McNeile (HPQCD), *PoS BEAUTY2016*, 069 (2016), [arXiv:1605.05645 \[hep-lat\]](#) .
- [74] B. Colquhoun, C. Davies, J. Koponen, A. Lytle, and C. McNeile (HPQCD), *PoS LATTICE2016*, 281 (2016), [arXiv:1611.01987 \[hep-lat\]](#) .
- [75] A. Sirlin, *Nucl. Phys.* **B196**, 83 (1982).
- [76] E. S. Ginsberg, *Phys. Rev.* **171**, 1675 (1968), [Erratum: *Phys. Rev.* **174**, 2169 (1968)].
- [77] D. Atwood and W. J. Marciano, *Phys. Rev.* **D41**, 1736 (1990).
- [78] J. D. Richman and P. R. Burchat, *Rev. Mod. Phys.* **67**, 893 (1995), [arXiv:hep-ph/9508250 \[hep-ph\]](#) .
- [79] A. Hart, G. M. von Hippel, and R. R. Horgan (HPQCD), *Phys. Rev.* **D79**, 074008 (2009), [arXiv:0812.0503 \[hep-lat\]](#) .
- [80] B. Chakraborty, C. T. H. Davies, P. G. de Oliveira, J. Koponen, G. P. Lepage, and R. S. Van de Water (HPQCD), *Phys. Rev.* **D96**, 034516 (2017), [arXiv:1601.03071 \[hep-lat\]](#) .
- [81] C. McNeile, private communication (2015).
- [82] R. J. Dowdall, C. T. H. Davies, G. P. Lepage, and C. McNeile (HPQCD), *Phys. Rev.* **D88**, 074504 (2013), [arXiv:1303.1670 \[hep-lat\]](#) .
- [83] C. T. H. Davies, E. Follana, I. D. Kendall, G. P. Lepage, and C. McNeile (HPQCD), *Phys. Rev.* **D81**, 034506 (2010), [arXiv:0910.1229 \[hep-lat\]](#) .
- [84] G. C. Donald, C. T. H. Davies, J. Koponen, and G. P. Lepage (HPQCD), *Phys. Rev.* **D90**, 074506 (2014), [arXiv:1311.6669 \[hep-lat\]](#) .
- [85] G. P. Lepage, B. Clark, C. T. H. Davies, K. Hornbostel, P. B. Mackenzie, C. Morningstar, and H. Trotter, *Nucl. Phys. Proc. Suppl.* **106**, 12 (2002), [arXiv:hep-lat/0110175 \[hep-lat\]](#) .
- [86] “Corrfitter,” <https://github.com/gplepage/corrfitter> (2018).
- [87] C. T. H. Davies, C. McNeile, E. Follana, G. P. Lepage, H. Na, and J. Shigemitsu (HPQCD), *Phys. Rev.* **D82**, 114504 (2010), [arXiv:1008.4018 \[hep-lat\]](#) .
- [88] S. Naik, *Nucl. Phys.* **B316**, 238 (1989).
- [89] M. E. Luke, *Phys. Lett.* **B252**, 447 (1990).
- [90] A. F. Falk and M. Neubert, *Phys. Rev.* **D47**, 2965 (1993), [arXiv:hep-ph/9209268 \[hep-ph\]](#) .
- [91] T. Mannel, *Phys. Rev.* **D50**, 428 (1994), [arXiv:hep-ph/9403249 \[hep-ph\]](#) .
- [92] A. Czarnecki, *Phys. Rev. Lett.* **76**, 4124 (1996), [arXiv:hep-ph/9603261 \[hep-ph\]](#) .
- [93] F. E. Close, G. J. Gounaris, and J. E. Paschalis, *Phys. Lett.* **149B**, 209 (1984).
- [94] A. Bazavov *et al.* (Fermilab Lattice, MILC, TUMQCD), *Phys. Rev.* **D98**, 054517 (2018), [arXiv:1802.04248 \[hep-lat\]](#) .
- [95] N. Brambilla, J. Komijani, A. S. Kronfeld, and A. Vairo (TUMQCD), *Phys. Rev.* **D97**, 034503 (2018), [arXiv:1712.04983 \[hep-ph\]](#) .
- [96] J. Laiho and R. S. Van de Water, *Phys. Rev.* **D73**, 054501 (2006), [arXiv:hep-lat/0512007 \[hep-lat\]](#) .
- [97] C. Bernard and D. Toussaint (MILC), *Phys. Rev.* **D97**, 074502 (2018), [arXiv:1707.05430 \[hep-lat\]](#) .
- [98] A. V. Avilés-Casco, C. DeTar, A. X. El-Khadra, A. S. Kronfeld, J. Laiho, and R. S. Van de Water, *PoS LATTICE2018*, 282 (2018), [arXiv:1901.00216 \[hep-lat\]](#) .
- [99] E. McLean, C. T. H. Davies, A. T. Lytle, and J. Koponen (HPQCD) (2018) [arXiv:1901.04979 \[hep-lat\]](#) .
- [100] M. Neubert, *Phys. Rept.* **245**, 259 (1994), [arXiv:hep-ph/9306320 \[hep-ph\]](#) .